MATERIALS PERFORMANCE OF STRUCTURAL ALLOYS IN CO_2 AND IN CO_2-STEAM ENVIRONMENTS

K. Natesan, Z. Zeng, and D. L. Rink
Argonne National Laboratory, 9700 South Cass Avenue, Argonne, IL 60439
E-mail: natesan@anl.gov; Telephone: (630) 252-5103; Fax: (630) 252-8681

Abstract

The U.S. Department of Energy (DOE) Office of Fossil Energy is intensely promoting research and development of oxy-fuel combustion systems that employ oxygen, instead of air, for burning the fuel. The resulting flue gas primarily consists of H_2O and CO_2 that facilitates sequestration of CO_2 or use it in a turbine to generate electricity, thereby leading to reduction in CO_2 emissions. Also, as the oxidant is bereft of N_2, NO_x emissions are minimized to a great extent from the exhaust gas. Studies at NETL have indicated that oxy-fuel combustion can increase efficiency in the power plants from the current 30-35% to 50-60%. However, the presence of H_2O/CO_2 and trace constituents like sulfur and chlorine in the gas environment and coal ash deposits at the operating temperatures and pressures can have adverse effects on the corrosion and mechanical properties of structural alloys. Thus, there is a critical need to evaluate the response of structural and turbine materials in simulated H_2O/CO_2 environments in an effort to select materials that have adequate high temperature mechanical properties and long-term environmental performance.

As a first step, we have evaluated the corrosion performance of the materials in CO_2, steam, and in steam-CO_2 mixtures. Materials selected for the study include intermediate-chromium ferritic steels, Fe-Cr-Ni heat-resistant alloys, and nickel-based superalloys. Coupon specimens of several of the alloys were exposed to pure CO_2 and to CO_2 plus steam environments at temperatures between 650 and 950°C for times up to 10,000 h. Detailed results are presented on weight change, scale thickness, internal penetration, microstructural characteristics of corrosion products, mechanical integrity and cracking of scales for the several structural alloys after long term exposure at 750°C. The information is used to address the long-term performance of the alloys for use in oxy-fuel combustion environments. In the future experiments, it is planned to incorporate low levels of sulfur and chlorine compounds (in addition to CO_2 and steam) in the exposure environment to establish the role of second/third reactant on the scaling, internal penetration, and long term performance of the structural alloys.

Background

An increase in carbon dioxide gas in the atmosphere is identified as one of the major causes for the global climate change and one of the sources of carbon dioxide is the exhaust from fossil fuel fired combustion power plants. The energy production, in particular electricity generation, is expected to increase globally due to population increase and per capita increase in energy consumption. To meet the energy needs, fossil fuels (coal, oil, and gas) will play a major part in production even with a projected increase in alternate renewable sources. However, to minimize the carbon dioxide emission, the current systems emphasize its capture from power plants and subsequent sequestration. The oxy-fuel combustion systems (without the diluent nitrogen gas) can enable recycling of the carbon dioxide to the compressor, use of novel gas turbines, and advance reuse.

The U.S. department of Energy/Office of Fossil Energy is supporting the development of combustion systems replacing air with nearly pure oxygen with a goal to achieving a near zero-emission coal-based power system. For this purpose turbines and combustor technologies that use pure oxygen in fuel combustion are being developed. The major advantage of combustion under pure oxygen is the potential for separation and capture of CO_2 and for achieving power system efficiencies in the range of 50 to 60%.

The objective of this phase of the work is to evaluate the oxidation and corrosion performance of structural and gas turbine alloys in CO_2 and steam/CO_2 environments over a wide temperature range. Further, the goal is to establish the kinetics of scaling and internal penetration, if any, and develop correlations for long-term performance of the alloys. Eventually, the influence of other reactants such as, sulfur and chlorine as well as presence of coal ash in the exposure environment on the corrosion and mechanical properties of the candidate alloys needs evaluation.

Experimental Procedure

Materials

The compositions of the alloys selected for the study are listed in Table 1. Several alloys, both ASME coded and uncoded, were selected for corrosion evaluation. The alloys included advanced ferritic steel modified 9Cr-1Mo and austenitic Fe-base alloys Types 304 and 330 stainless steel and Alloy 800H. In addition, several high-Ni alloys (333, 617, 625, 602CA, 230, 693, 740, and 718) were included in the study, especially for application at temperatures above 700°C. MA956 is a Fe-Cr alloy produced via mechanical alloying and subsequent extrusion.

Apart from fireside and steam side corrosion resistance, the alloy selected for application in steam superheaters and reheaters should possess adequate strength at elevated temperatures for the duration of service. Figure 1 shows a compilation of ASME Code allowable stress values as a function of temperature. Figures 1(a) and 1(b) show the stress values for 460-900°C and 650-800°C, respectively. Alloys such as 693, 740, and MA956 are not Code certified and their stress values are not shown in the figures. However, laboratory creep test data indicate that Alloy 740 has higher strength than 617 or 230.

Table 1. Nominal composition (in wt.%) of alloys selected for corrosion study

Material	C	Cr	Ni	Mn	Si	Mo	Fe	Other
Modified 9Cr	0.10	9.0	0.8	0.5	0.4	1.0	Bal	Nb 0.08, V 0.20, N 0.06
304	0.08	18.0	8.0	1.6	0.6	-	Bal	
800H	0.08	20.1	31.7	1.0	0.2	0.3	Bal	Al 0.4, Ti 0.3
330	0.05	10.0	35.0	1.5	1.25	-	Bal	
333	0.05	25.0	45.0	-	1.0	3.0	18.0	Co 3.0, W 3.0
617	0.08	21.6	53.6	0.1	0.1	9.5	0.9	Co 12.5, Al 1.2, Ti 0.3
625	0.05	21.5	Bal	0.3	0.3	9.0	2.5	Nb 3.7, Al 0.2, Ti 0.2
602CA	0.19	25.1	62.6	0.1	0.1	-	9.3	Al 2.3, Ti 0.13, Zr 0.19, Y 0.09
230	0.11	21.7	60.4	0.5	0.4	1.4	1.2	W 14, Al 0.3, La 0.015
693	0.02	28.8	Bal	0.2	0.04	0.13	5.8	Al 3.3, Nb 0.67, Ti 0.4, Zr 0.03
740	0.07	25.0	Bal	0.3	0.5	0.5	1.0	Co 20.0, Ti 2.0, Al 0.8,, Nb+Ta 2.0
718	-	19.0	52.0	-	-	3.0	19.0	Nb 5.0, Al 0.5, Ti 0.9, B 0.002
MA956	-	20.0	-	-	-	-	Bal	Al 4.5, Ti 0.5, Y_2O_3 0.6

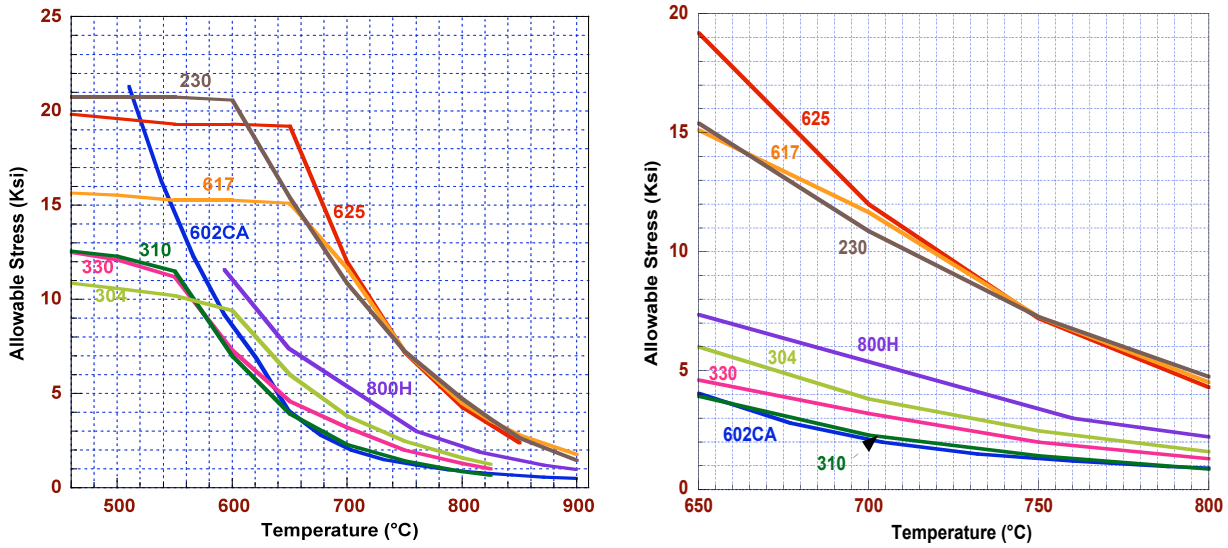

Figure 1. Code allowable stress as a function of temperature for various structural alloy candidates for the temperature range (a) 460-900°C and (b) 650-800°C.

Two different experimental systems were used for the oxidation in CO_2 and in steam-CO_2 environments. Details on the experimental facilities and procedures used in oxidation studies were presented in earlier papers (1, 2). Upon completion of the exposures, the specimen surfaces were analyzed using a scanning electron microscope equipped with an energy dispersive X-ray analyzer. The specimens were electrolytically etched with 10% acetic acid at 10 V for 30 seconds, to evaluate the internal penetration of the substrate alloy using optical metallography. In addition to weight change in specimens, microscopy of the cross sections of the exposed specimens was used to establish the internal penetration, if any, into the substrate of various specimens. Some of the specimens were also examined in detail using Raman spectroscopy and synchrotron X-ray analysis.

Results and Discussion

Corrosion Performance

Specimens of various alloys were exposed to pure CO_2, 50% CO_2-steam, and air at 750°C and in pure steam at 725°C, for times up to 10,090 h. Figure 2 (a-d) show the weight change data for the alloys after exposure in various environments. The data show that the weight change for all the alloys is small when tested in all four environments. Among the alloys, Alloy 800 exhibited the most weight gain all four environments. In general, high nickel and Ni-base alloys exhibited less oxidation than the Fe-base alloys in all exposure environments. The high silicon alloys such as Alloys 330 and 333 showed superior corrosion resistance in pure CO_2 environment when compared their performance in CO_2-steam or pure steam environments. The volatilization of silicon oxides in steam-containing environments may be the cause for this increased corrosion. Figure 3 shows a plot of the relative stability of various oxide and spinel phases as a function of temperature. Also shown in the figure are the oxygen partial pressures established by the CO_2 and

steam environments. It is evident that all the relevant (to alloy protection) oxide and spinel phases will be thermodynamically stable in both exposure environments. Therefore, the phases that form in the thermally grown scale will be influenced predominantly by the alloying elements present in the alloy rather than by the oxygen partial pressure in the exposure environment.

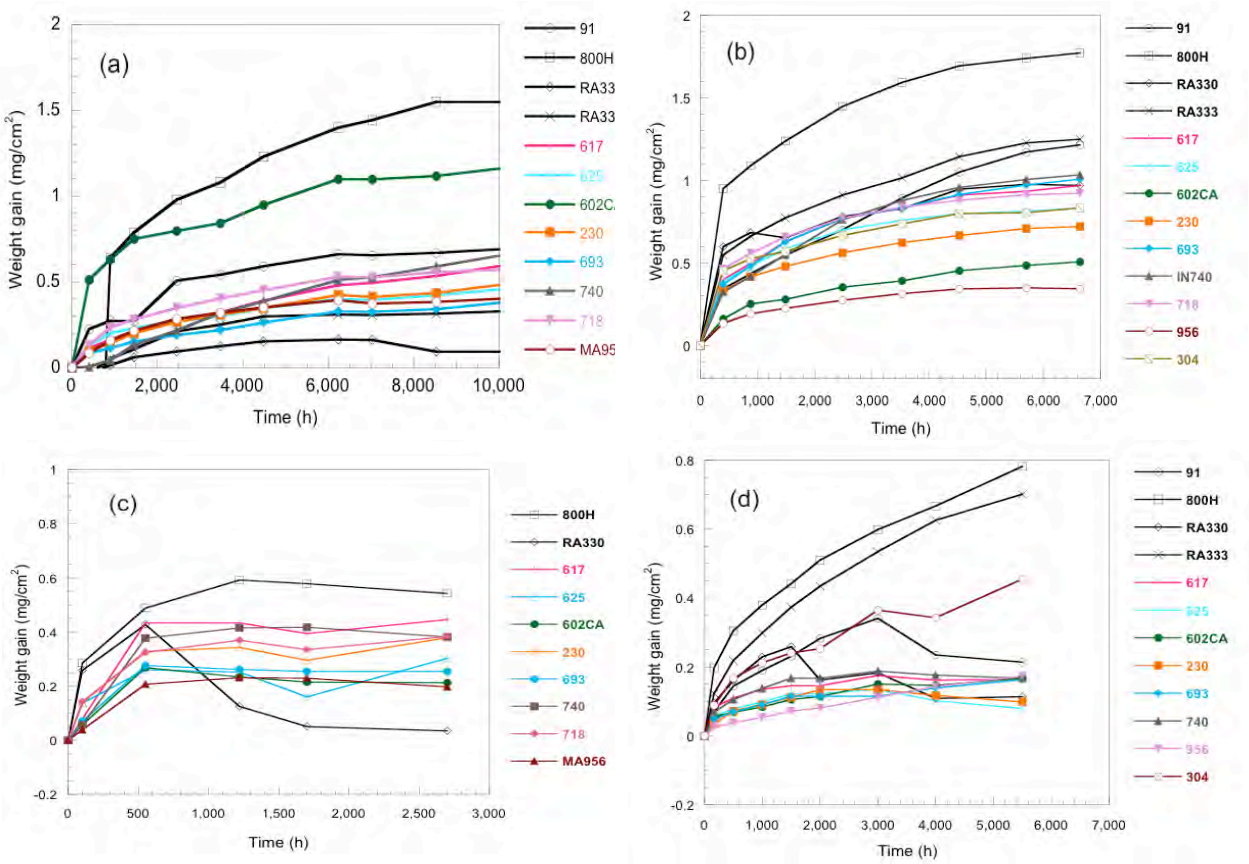

Figure 2. Weight change data for structural alloys after testing in (a) pure CO_2, 750°C, (b) 50% CO_2-50% steam, 750°C, (c) pure steam, 725°C, and (d) air, 750°C.

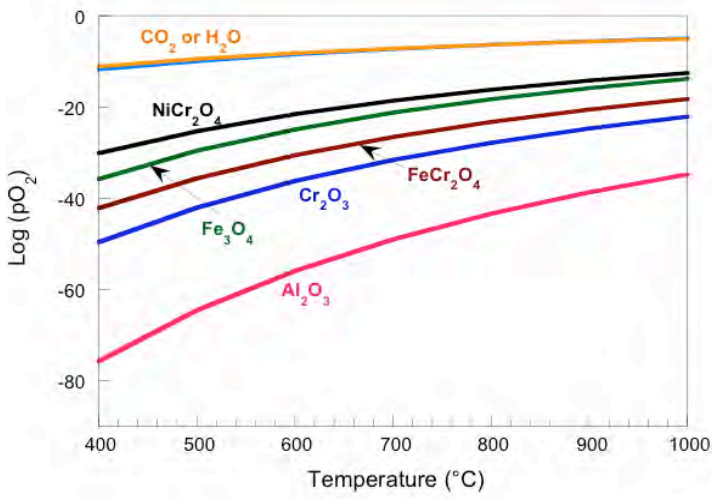

Figure 3. Thermodynamic stability of various oxide and spinel phases. Also shown are the pO_2 curves for pure CO_2 and pure steam.

Figure 4 shows a comparison of weight change data for individual alloys after exposure in the four different environments. In general, all alloys, except 602CA, show the highest oxidation rates in 50% CO_2-50% steam environment. The data also indicate a linear rate (after initial weight gain) for all nickel base alloys exposed to pure CO_2 environment. On the other hand, the alloys exhibit a parabolic behavior in the CO_2-steam mixture. The data also show that substantial additional work is needed on the oxidation of these alloys in steam at atmospheric and at high pressures.

Microstructural Characterization of Oxide Scales

Phase composition of oxides could greatly affect the capability of alloys to resist continued degradation. In the early stage of oxide scale formation, nickel and cobalt in the alloy could oxidize to 2+ at the gas-oxide surface and dope into the solid solution of $(Fe,Ni,Co)Cr_2O_4$. When cations continue to diffuse out, the nickel and cobalt containing spinel is buried inside. The pO_2 in the inner layer of the oxide scale decreases with increasing thickness of the oxide scale, and Ni^{2+} and Co^{2+} will be reduced to nickel metal when the pO_2 drops below the critical value. Such a process leads to the formation of nickel and cobalt particles in oxide scale. $FeCr_2O_4$ spinel itself is not stable either. Iron ions can also be reduced to metallic particles in the oxide scale. Therefore, formation of the metallic nanoparticles can occur due to the reduction of nickel, cobalt, and iron ions in the spinel phase during the growth of the oxide scale (3).

Spinel and chromium oxide phases were observed by Raman scattering. The reduction of spinel could lead to the formation of metallic nanoparticles in oxide scale but the pO_2 is high enough that chromium oxide is not reduced. The distribution of spinel and chromium oxide phases in oxide scales could be useful to understand the degradation of the oxide scales. We used Raman mapping technique to study the distribution of spinel and chromium oxide phases in the oxide scale on Alloy 617. Figure 5 shows that the distribution of chromium oxide and spinel are not uniform. The intensities of the Raman scattering of chromium oxide at the damaged areas are weak, whereas Raman scatterings from spinel were strong. SEM analysis showed metal particles at the damaged areas. Metallic network may form when the spinel phase decomposes at low pO_2 during the growth of oxide scale. Nickel and iron metal particles were rejected to the grain boundary regions (of oxide) with grain size of approximately several hundred nm. Metal particles can connect in the grain boundary regions of the oxides and form a metallic network. Carbon could diffuse through these metallic networks and enter the underlying substrate alloy. Chromium mobility will be limited after formation of chromium carbide, which may lead to less protection of alloy from oxidation and nodular corrosion.

Figure 6 shows SEM photomicrographs of cross sections of Alloy 625 after exposure in the four different environments. Dense and uniform oxide scales were observed on the specimens exposed to pure CO_2, 50% CO_2–50% steam, and air environments at 750°C. The alloy exhibited nodular degradation when exposed to pure steam. The nodular region also showed fine distribution of metallic nanoparticles. Among the four environments used in these tests, exposure to pure steam resulted in significant amount of metal nanoparticles in oxide scales developed on many of the alloys.

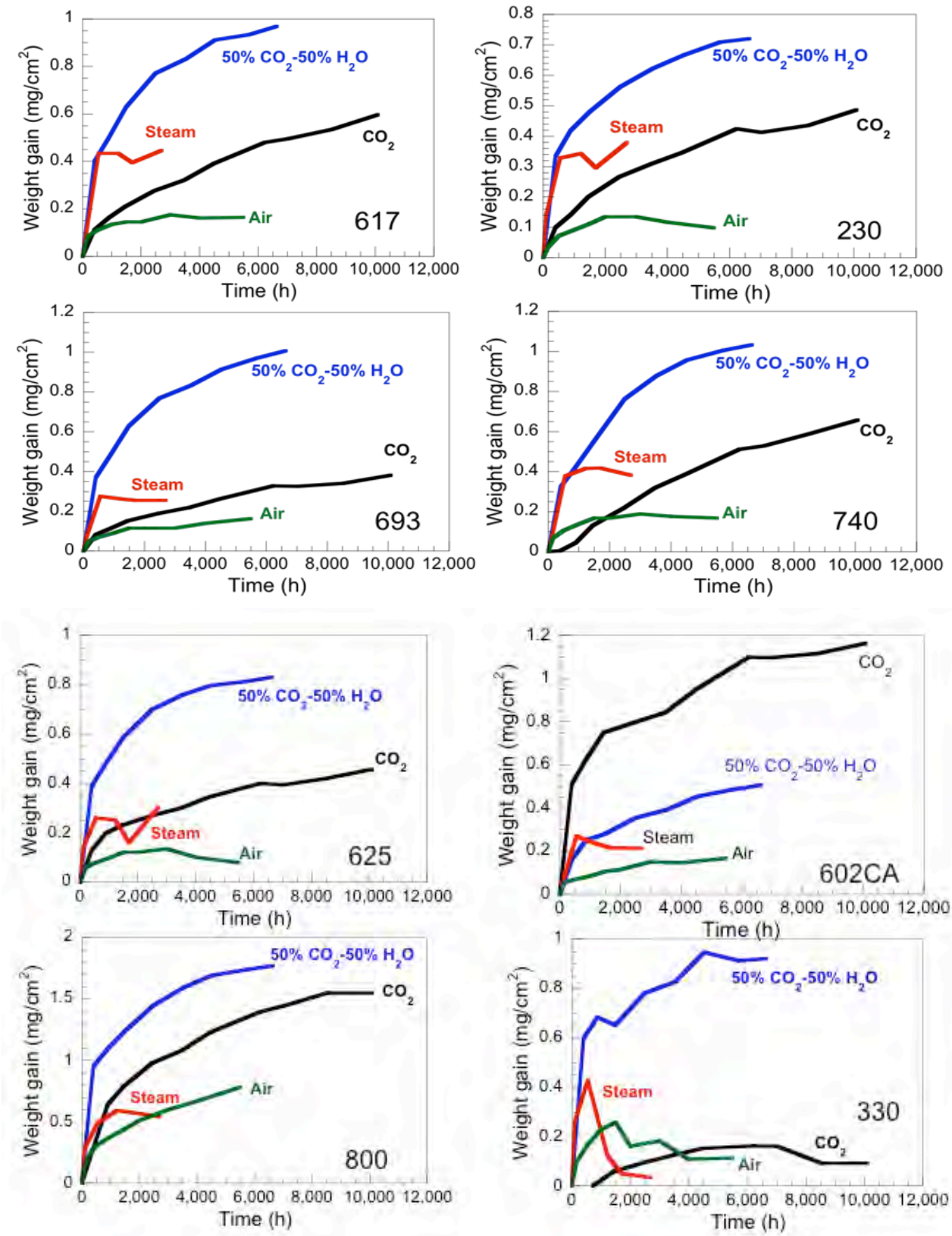

Figure 4. The effect of exposure environment on the weight change data for individual alloys at 750°C, except for tests in steam conducted at 725°C.

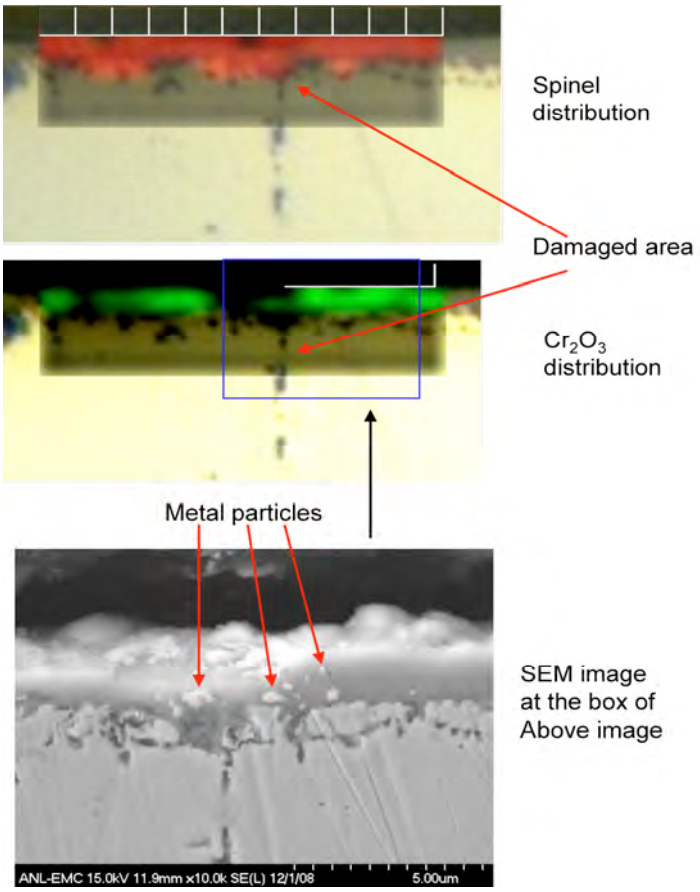

Figure 5. Raman mapping of spinel and Cr_2O_3 and the SEM image at the damage area of Alloy 617 after 1330-h exposure to pure CO_2.

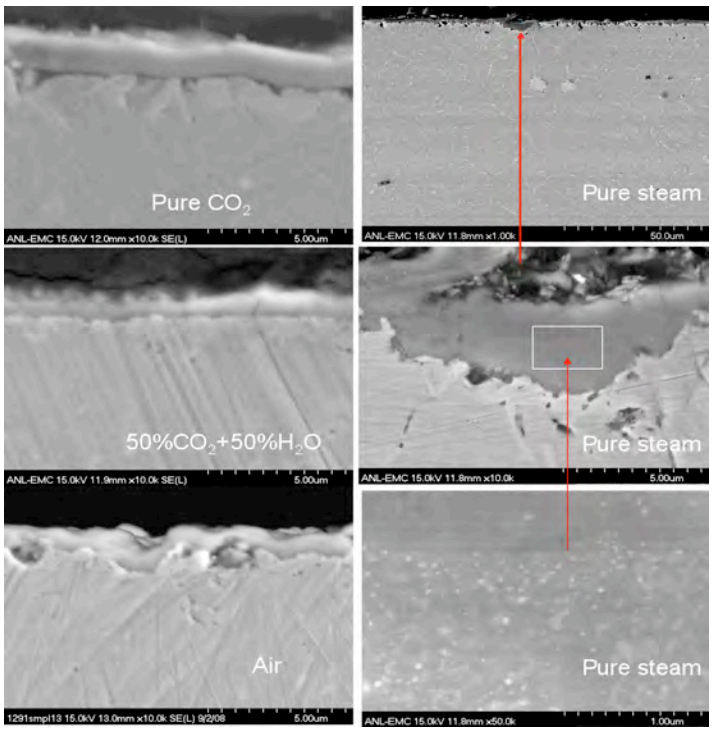

Figure 6. SEM cross sections of Alloy 625 that were exposed to pure CO_2, pure steam, 50% CO_2–50% steam, and air environments at 750°C. The right column shows the damage location in steam.

When the alloys were tested in pure CO_2, similar effect of metallic networks on the alloy degradation was observed. Metallic nanoparticles were generally observed in oxide scales developed in alloys with high rate of internal penetration or larger scale thickness, whereas, metallic nanoparticles were not seen in scales developed on Alloys 625 and MA956 even after 10,090-h exposure to pure CO_2 at 750°C (see Fig. 7).

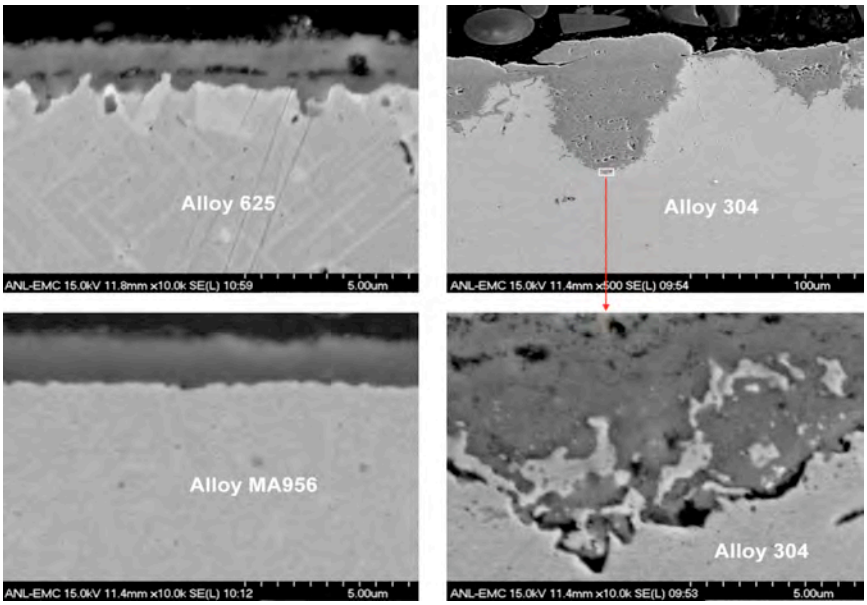

Figure 7. SEM images for Alloys 625, MA956, and 304 stainless steel tested in pure CO_2 at 750°C for 10,090 h. The magnified image of 304 shows metallic networks in the locally damaged area of the oxide.

Raman analysis of the scales showed that the peak width of Raman scattering is related to the crystalline size and disordering of the grains in oxide scales. The wide Raman peak usually indicates that the grains of oxides are disordered. The Raman peak of Cr_2O_3 in oxide scale for the Alloy 617 specimen after exposure to pure CO_2 is much wider than that after exposure to air (Fig. 8), indicating that the oxide grains after exposure to CO_2 and steam are highly disordered. The disordered Cr_2O_3 doesn't seem to protect the alloy, resulting in thicker scale. Weight gains for Alloys 617, 602CA, and 625 after exposure to air are the smallest, which also indicates that the better crystallinity of Cr_2O_3 in these scales may be important to protect the alloys from degradation at high temperatures.

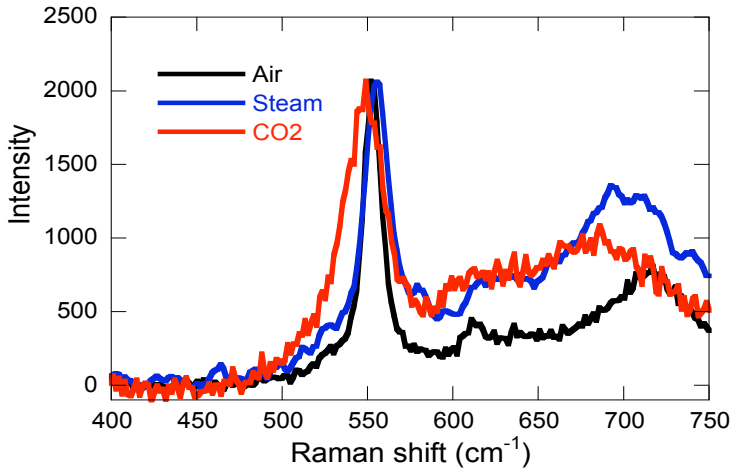

Figure 8. Raman spectra on oxide scale of Alloy 617 after exposure to Air, steam, and pure CO_2 at 750°C.

Scaling and Internal Penetration Rates

The exposed specimens were also analyzed to evaluate the total corrosion (scale thickness and penetration) for all the alloys after exposure at 750°C in pure CO_2 and in 50% CO_2–50% steam. Figure 9 shows the scale and penetration rates for several alloys tested at 750°C in 50% CO_2–50% steam environment, assuming a parabolic kinetics. Results showed that all of the alloys exhibit total corrosion rate of <0.05 mm/y at 750°C. The measured corrosion rates include penetration depth values that were observed in the pits and represent maximum rates for these alloys. Figure 10 shows the ratio of penetration depth to scale thickness observed for alloys tested at 750°C in 50% CO_2–50% steam and in pure CO_2. The data indicate that the penetration rates are much grater than the scaling rates (ratio being >1) and such increased penetration of the alloy can affect the long-term mechanical property (such as creep and creep fatigue) of the structural components.

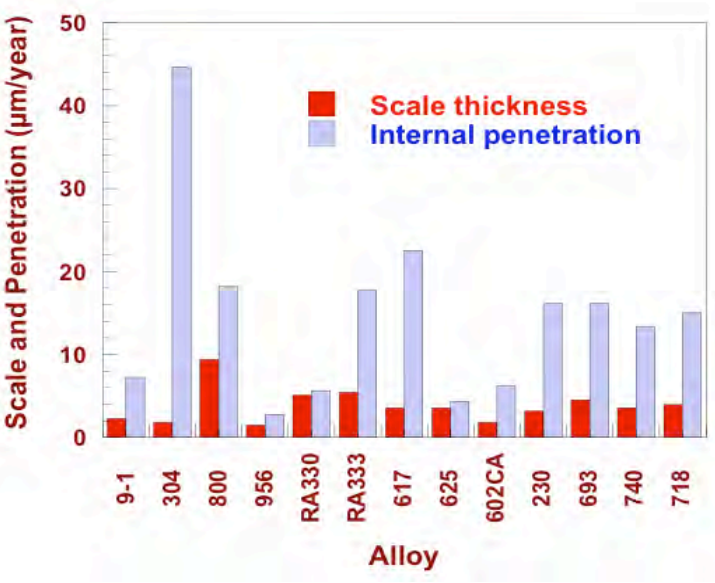

Figure 9. Scale and penetration rates for alloys tested in 50% CO_2-50% steam at 750°C.

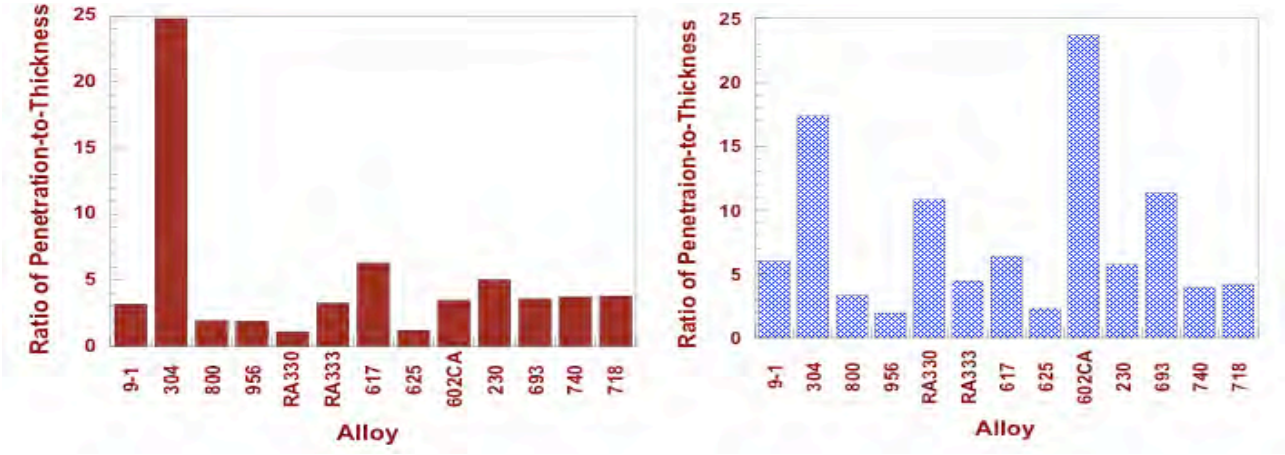

(a) (b)

Figure 10. Ratio of penetration depth to scale thickness for alloys exposed at 750°C to (a) 50% CO_2-50% steam and (b) pure CO_2.

Figure 11 shows the effect of exposure time on the relative alloy penetration rate to the scaling rate for the alloys exposed to pure CO_2 environment. The results show that the internal penetration rates are much larger than the scaling rates for most of the alloys. The penetration-to-thickness ratios for alloys MA956, 740 and 718 are close to 1, indicating that scaling and penetration rates are almost time independent and both progress at the same rates. Many of the other alloys exhibit penetration-to-thickness ratios >1 with increased exposure time, and this may have implications on the long-term mechanical properties of the alloys. In such cases, a simple corrosion allowance to account for metal wastage may not be realistic to assess and account for the corrosion degradation.

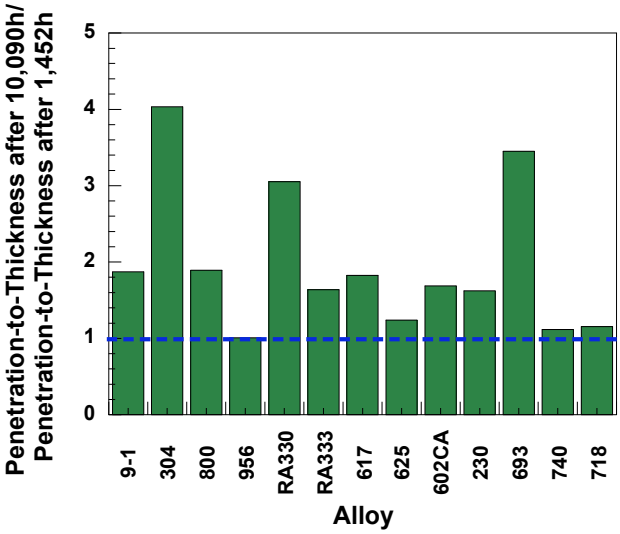

Figure 11. A comparison of the ratio of penetration depth to scale thickness for alloys exposed for 1,452 and 10,090 h in pure CO_2 at 750°C.

Summary

At Argonne National Laboratory, we have conducted a study to evaluate the oxidation performance of structural alloys in several environments that include, pure CO_2 and CO_2-steam, pure steam, and air at temperatures up to 950°C. We have selected several structural alloys and limited turbine alloys and will incorporate additional gas-turbine alloys as they become available. We have presented the results obtained on the corrosion performance of various alloys after exposure at 750°C. We have addressed the mechanism for the oxidation of various alloys in these environments and also evaluated the long-term performance of the alloys from the standpoint of scaling and internal penetration. The oxidation test results showed that the total corrosion (scaling plus internal penetration) rates are <0.05 mm/y at 750°C. Substantial additional long-term data are being developed for several of the alloys after exposure in the presence of coal ash and flue gas environments to quantify the role of corrosion-accelerating agents such as sulfur, chlorine, and alkalis.

Acknowledgements

This work was supported by the U.S. Department of Energy, Office of Fossil Energy, Advanced Research Materials Program, Work Breakdown Structure Element ANL–4, under Contract DE-AC02-06CH11357.

References

1. K. Natesan and D. L. Rink, "Corrosion Performance of Structural Alloys for Oxy-fuel Combustion Systems," Proc. 21st Annual Conference on Fossil Energy Materials, Knoxville, TN, April 30- May 2, 2007.

2. K. Natesan, Z. Zeng, and D. L. Rink, "Materials Performance of Structural Alloys in CO_2 and in CO_2-Steam Environments," Proc. 22nd Annual Conference on Fossil Energy Materials, Pittsburgh, PA, June 8-10, 2008.

3. Z. Zeng, K. Natesan, Z. Cai, and S. B. Darling, "The role of metal nanoparticles and nanonetworks in alloy degradation," *Nature Materials*, **7**, (2008) 641–646.